ACADEMIA QUANTUM

Research Article
Published: 2025-06-27
https://doi.org/10.20935/AcadQuant7780

Detection of 5 GHz photons using Al Josephson junctions at 0.7 K

Dmitry A. Ladeynov[1,2], Andrey L. Pankratov[1,2,3,*], Leonid S. Revin[1,3], Anna V. Gordeeva[1], Alexander V. Chiginev[1,3], Sergey A. Razov[1], Eugeny V. Il'ichev[4]

Academic Editor: Yuhua Duan

Abstract

We predict that threshold detectors based on Al Josephson junctions with critical currents below 100 nA exhibiting a phase diffusion regime can be exploited for microwave photon detection at both 17 mK and 700 mK. We demonstrate the detection of two- and one-photon energies at 5 GHz with 90% and 15% efficiency and dark count times of about 0.1 s and 0.01 s, respectively. The weak temperature dependence of the detector's performance observed in the sub-kelvin range fully confirms its phase diffusion mode of operation. On the other hand, these results show that inevitable thermal fluctuations are not the main source of detector noise. Consequently, there is still room to optimize the detector's performance. These results are important for axion search experiments in the range of 5–25 GHz (20–100 μeV).

Keywords: *Josephson threshold detector, RCSJ model, noise-induced escape, microwave photons*

Citation: Ladeynov DA, Pankratov AL, Revin LS, Gordeeva AV, Chiginev AV, Razov SA, et al. Detection of 5 GHz photons using Al Josephson junctions at 0.7 K. *Academia Quantum* 2025;2. https://doi.org/10.20935/AcadQuant7780

1. Introduction

Modern developments in quantum communications and quantum information processing devices have benefited greatly from the efficient detection of individual photons. However, the widely used conventional single-photon detectors, such as superconducting nanowires [1, 2] and transition-edge devices [3–5], require a sufficiently high incident photon energy to modify the state of the detector. In the microwave frequency range, the corresponding energy is rather low, at about 10 yJ. Consequently, practicable single-photon detectors for the microwave field have not yet been implemented. A natural idea for realizing such a detector is exploiting quantum Josephson circuits. Indeed, superconducting qubits, being two-level quantum systems with a characteristic energy within the microwave scale, can be excited through the absorption of an incident photon. Various types of qubit- and quantum-dot-based photon detectors have been proposed and implemented [6–18], with efficiencies approaching ≈60% [11, 16].

As a photon detector, we use a current-biased Josephson junction (CBJJ), which has also been utilized before as the phase qubit [19]. The Josephson phase across the junction for such devices is associated with the dynamics of a "particle" in a washboard potential [20]; see **Figure 1a**. In the detector's initial state, corresponding to a zero-voltage state, the particle is trapped in one of the local minima of the potential. After the incident microwave field delocalizes the trapped particle, it escapes into the "running state" (RS), providing a finite voltage across the CBJJ. This voltage is in the millivolt range and can easily be measured.

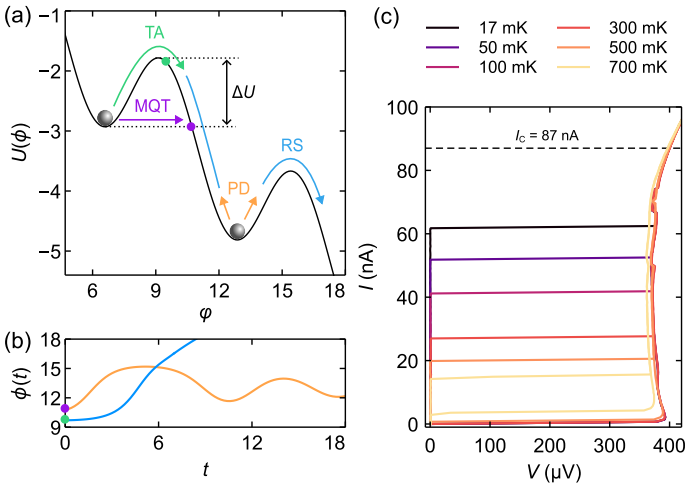

Figure 1 • Phase particle regimes and current–voltage characteristics (IVCs). (**a**) Regimes under tilted potential. Here, TA refers to thermal activation, MQT to macroscopic quantum tunneling, RS to switching to the running state with a finite voltage, and PD to the phase diffusion regime with re-trapping. (**b**) Phase evolution. If a particle escapes due to TA, it gains more potential energy (green dot) and thus has a higher probability of RS. If a particle tunnels under the barrier (violet dot), it has a lower potential energy and a higher probability of being re-trapped, leading to quantum PD. (**c**) IVCs of SIS3; the dashed line is the theoretical critical current.

[1]Nizhny Novgorod State Technical University n. a. R. E. Alekseev, Nizhny Novgorod 603155, Russia.
[2]Institute of Information Technology, Mathematics and Mechanics (IITMM), N. I. Lobachevsky State University of Nizhny Novgorod, Nizhny Novgorod 603022, Russia.
[3]Institute for Physics of Microstructures of the Russian Academy of Sciences, Nizhny Novgorod 603950, Russia.
[4]Leibniz Institute of Photonic Technology, Jena, D-07702, Germany.
*email: alp@ipmras.ru

However, to realize the maximum sensitivity, the CBJJ must be biased relatively close to the critical current value. Due to fluctuations, such initialization causes uncontrolled transitions into a voltage state, corresponding to the dark count rate. The trade-off between the initialization point and resolution, which is common for threshold-type detectors, is clearly seen for this particular realization [21]. In fact, this is the main obstacle to implementing an efficient single-photon detector for the microwave range. Importantly, the relatively long lifetime of the threshold detector in the initial (zero-voltage) state is a key issue for dark matter axion-type particle searches [22–34]. Moreover, it was recently predicted [35] that one of the most interesting ranges for an axion search is 20–100 μeV, corresponding to the 5–25 GHz range, covered by the detectors considered here.

Various approaches to optimizing CBJJ threshold detectors have been used [36–46]. Interestingly, the theoretically estimated lifetimes in the zero-voltage state for the threshold detectors studied have been substantially shorter than the experimentally measured ones. To explain this inconsistency, it has been proposed that the CBJJ is in the so-called phase diffusion regime [47].

The main feature of the phase diffusion (PD) regime can be commented on, in a hand-waving manner, as follows. After the escape from the initial minimum of the washboard potential, as shown in **Figure 1a**, via thermal activation (TA) or macroscopic quantum tunneling (MQT), the phase can be re-trapped into another minimum with a relatively high probability—see **Figure 1b**—where the phase evolution is calculated numerically using the Resistively and Capacitively Shunted Junction (RCSJ) model [20]. Consequently, in the PD regime, the CBJJ very rarely switches to the voltage state due to re-trapping, which effectively increases its lifetime in the initial state. However, for the case of an arriving photon, switching into the running state without re-trapping may occur due to the induced current pulse, which significantly exceeds the detector's threshold. While the main characteristics of the phase diffusion regime have been well described [48–58], its application to photon counting is a relative unknown. In this paper, after a detailed investigation of the switching dynamics of CBJJs, we demonstrate single- and double-photon detection at 5 GHz with an efficiency of about 15% and 90%, respectively. Importantly, increasing the temperature more than 40 times over (from 17 mK to 700 mK; see below) does not lead to degradation of the detector's performance for a properly chosen sample. In practice, this counter-intuitive result means that inevitable thermal fluctuations can be "compensated for" by the phase diffusion mechanism.

2. Materials and methods

2.1. The theoretical model

The switching processes in a CBJJ can be described according to the dynamics of a phase "particle" of a mass C (capacitance) moving under the effect of damping $1/R$ (with the normal state resistance R) under a tilted periodic potential $U(\phi) = -E_J(i\phi + \cos\phi)$—see **Figure 1a**—according to the RCSJ model. Here, ϕ is the Josephson phase, and $E_J = \hbar I_C/(2e)$ is the Josephson energy, with the CBJJ's critical current I_C, the reduced Planck constant $\hbar$, the electron charge e, and the normalized bias current $i = I/I_C$. Previously, we described several scenarios (MQT, RS, PD) of phase behavior [59]. The transition to these scenarios is connected with the phase particle dynamics escaping from a potential well. This well is metastable due to the effect of noise, and the particle can escape across the barrier due to TA or tunnel through the barrier at lower temperatures (MQT).

The survival time in a potential well (the lifetime) is described using the following set of approximate expressions τ_{TA} (the TA regime, Kramers) and τ_Q (the MQT regime) [59–62]:

$$\begin{cases} \tau_{TA} = \dfrac{2\pi}{\omega_0} a_{TA}^{-1} e^{\frac{\Delta U}{k_B T}}, T \geq T_Q \\ \tau_Q = \dfrac{2\pi}{\omega_0}\sqrt{\dfrac{2\pi}{B}} e^{B}, \; T < T_Q \end{cases} \quad (1)$$

where T_Q is the quantum crossover temperature, $\omega_0 = \omega_p\left(1-i^2\right)^{1/4}$ is the oscillation frequency around the bottom of the well, $\omega_p = \sqrt{2eI_C/\hbar C}$ is the plasma frequency, $\Delta U(i) = 2E_J\left[\sqrt{1-i^2} - i\arccos i\right]$ is the barrier height of a potential with a localized phase particle, and k_B is the Boltzmann constant. Here, $a_{TA} = 4/\left(\sqrt{1+Qk_BT/(1.8\Delta U)}+1\right)^2$, $B = (\Delta U[7.2+8A/Q])/(\hbar\omega_0)$ (with the numerical parameter A), and $Q = \omega_0 RC$. The probability density of switching currents was considered as $W(i) = -\partial P(i)/\partial i$, where the probability $P(i) = \exp\left(-I_v^{-1}\int_0^i {}^1/_{\tau(i')}\,di'\right)$ was derived from the adiabatic approximation [63], bearing in mind the slow change $I_v = \partial i/\partial t$ in bias sweep in comparison with the inversed plasma frequency.

2.2. The sample fabrication and experimental setup

The analysis of the CBJJ dynamics is carried out based on the experimental data for three samples of superconductor–insulator–superconductor (SIS) tunnel junctions: SIS1, with an area of 7 μm^2; SIS2, with an area of 2 μm^2; and SIS3, with an area of 0.8 μm^2, located on the same chip. See the diagram in **Figure 2** and the additional information in **Table 1**. Here, the critical currents of the samples are obtained by fitting the switching current distributions using theory **(1)**. It is known that the critical currents of small-area junctions are suppressed by MQT [43] compared to the expectations of the Ambegaokar–Baratoff expression. The samples were fabricated using the self-aligned shadow evaporation technique [47, 58, 64].

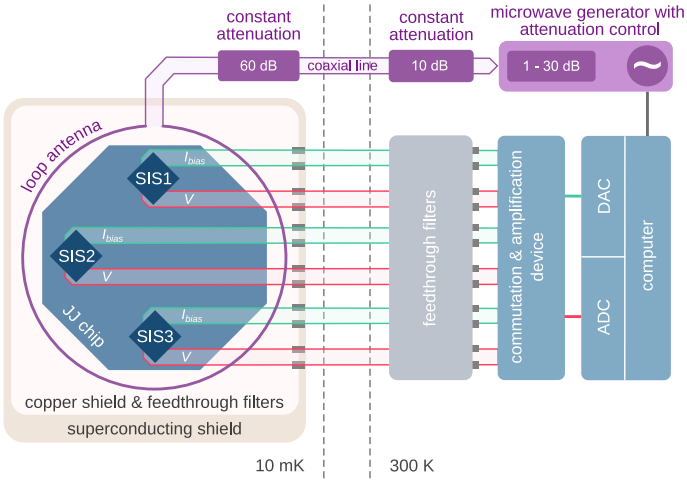

Figure 2 • Diagram of the experimental setup. Constant attenuators are distributed across a coaxial line as follows: 4 K plate—20 dB; 1 K plate—10 dB; 0.1 K plate—20 dB; 10 mK plate—10 dB.

Table 1 • Table of SIS parameters.

Sample	S (μm × μm)	I_C (nA)	R_N (KΩ)	C (fF)
SIS1	14 × 0.5	895	0.28	185
SIS2	2 × 1	270	1.05	100
SIS3	2 × 0.4	87	3.2	70

The CBJJ chip was thermally attached to the mixing chamber plate of a dry dilution refrigerator, providing a minimum nominal temperature of ∼12 mK with a temperature stability of ∼1 mK for operations below 1 K. The sample holder on a heavy copper leg for more efficient thermalization of the sample is surrounded by mu-metal and superconducting shields, in addition to the copper shield on a 1 K plate, decreasing the background radiation [65]. The superconducting shield has an additional thermal sink at its back edge to minimize the frozen magnetic field. To minimize low-frequency noise from the compressors and pumps, anti-vibration dampers were used. Well-filtered, twisted-pair lines were used for conventional four-point measurements. The experimental setup described, which was also used for single-photon detection by supplying a microwave signal via a coaxial cable inside the fridge, is shown in **Figure 2**.

3. Results

3.1. Switching current distributions

Measuring the switching statistics for a CBJJ from the zero-voltage state to the finite-voltage state in the temperature range between 15 mK and 1 K, the switching current distributions (SCDs) $W(I)$ were collected. To perform these measurements, a bias current applied to the junction was ramped up at a constant rate I_v with 5000 repetitions, so in the SCD plots, the error bars do not exceed the dot sizes. The ramp rates for each of the samples differ according to their sizes, so for SIS1, $I_v = 50$ nA/ms; for SIS2, $I_v = 20$ nA/ms; and for SIS3, $I_v = 5$ nA/ms.

An example of the current–voltage characteristic (IVC) for the SIS3 sample is shown in **Figure 1c**. Here, the theoretical critical current (87 nA, the dashed line) was restored by fitting through theory **(1)** using the CBJJ's normal state resistance and the temperature. Similarly, the critical currents for SIS1 and SIS2 were obtained as equal to 895 nA and 270 nA, respectively. Note that back-bending at the lower currents of the reverse IVC branch occurs due to weak local overheating of the sample and is visible for all measured samples. From the measurements of the switching current distributions—see **Figure 3**—we extract the mean switching current $\langle I_{sw}\rangle$, as well as the standard deviation σ, at various temperatures. Using the theory from the previous section, we reconstruct an approximation of the switching current distributions for SIS2. As can be seen in **Figure 3**, the MQT theory describes the behavior of the CBJJ, where thermal noise weakly affects its dynamics. In turn, the Kramers theory agrees well with the experimental results for the TA regime. Fitting the standard deviation curves using the $\sigma \sim T^{2/3}$ dependence [66] is an efficient tool for separating the CBJJ switching regimes, instead of recourse to detailed fitting, since this dependence (the yellow solid curve) actually coincides with the Kramers theory (the green dashed curve).

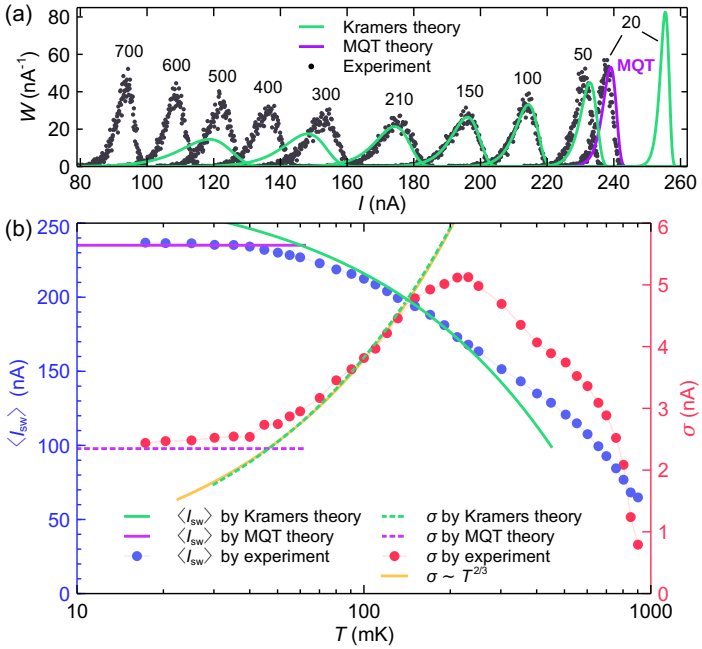

Figure 3 • The experimentally derived SCD for the SIS2 sample, compared with theory (1). (**a**) The switching current distributions $W(I)$ for various sample temperatures (marked in mK above each experimental curve). (**b**) The experimental values of the mean switching current and the standard deviation (blue and red circles) and theoretical estimates (solid and dashed curves).

Qualitatively, the dependence of the standard deviation versus temperature is similar for all samples—see **Figure 4**—and three main switching regimes for the CBJJ are clearly visible here. At low temperatures, MQT determines the dynamics of the detector. Indeed, below 50 mK, the $\sigma(T)$ dependence is saturated; see **Figure 4**. As the temperature increases, the growth of $\sigma(T)$ accelerates. This indicates the transition between the MQT regime and the dominating TA dynamics. Here, the dependence $\sigma(T)$ can be approximated using the function $T^{2/3}$ (see the green curves in **Figure 4**), known for TA switching [66]. Consequently, separation between the MQT and TA regimes (quantum crossover) is clearly visible. With a further increase in temperature, deviation from the TA behavior due to a transition to the phase diffusion regime is observed. In spite of the different nominal critical currents (87 nA, 270 nA, and 895 nA), all of these CBJJs demonstrate the transition to the phase diffusion regime (the point of deviation of $\sigma(T)$ from $T^{2/3}$ dependence); see **Figure 4**.

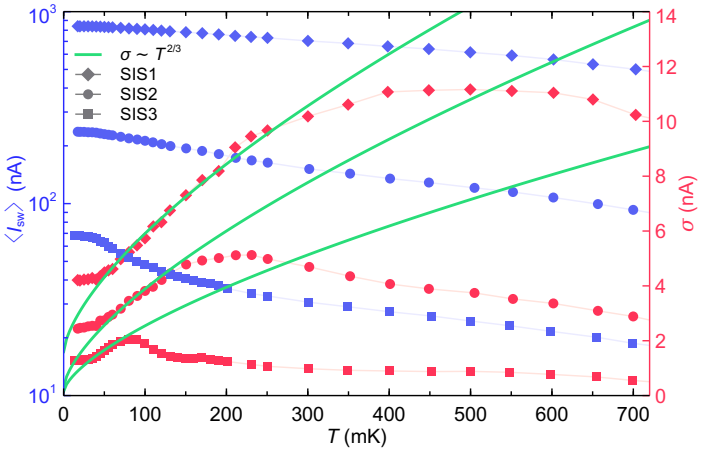

Figure 4 • The experimental values of the mean switching current and the standard deviation. The blue markers are the mean switching current $\langle I_{sw} \rangle$, and the red markers are the standard deviation σ. Green solid curves show the TA mechanism $\sigma \sim T^{2/3}$ [66].

3.2. Lifetimes

In addition to the switching current distributions, an important characteristic for microwave single-photon detector applications is the lifetime of the zero-voltage state (the dark count time) $\tau(T)$. In **Figure 5b,d,f**, the dark count time curves $\tau(T)$ are presented as a function of the bias current and temperature (shown in mK at each curve). Here, an important characteristic of the lifetime is not only its value at a certain bias current but also its tilt. It is obvious that for steeper tilts, taking the desired dark count time value, one can more closely approach the measured critical current (defined as $\langle I_{sw} \rangle$), thus decreasing the detection threshold and improving the sensitivity. Usually, it is assumed that the lifetime tilt increases with decreasing temperature, which is not always so, as we show below.

By making use of experimental data on $\sigma(T)$ (**Figure 5a,c,e**), we present the different switching regimes for the lifetimes $\tau(T)$ (**Figure 5b,d,f**). Areas of different types of switching are highlighted: MQT (the violet area), TA (the white area), and PD (the orange area). Essentially, all samples behave similarly and differ in the scale of each region only. A tendency here is visible in **Figure 5**: the lower the critical current of the sample, the narrower the white TA region, the broader the orange PD region, and the MQT area is reduced as well.

Usually, below T_Q, the lifetime can be predicted using the MQT theory [43, 59, 61], but for the quantum phase diffusion regime, some corrections are expected. Basically, quantum PD can manifest itself as an increase in lifetimes compared to those calculated using MQT theory. However, for CBJJs with high critical currents, the quantum PD effect was not demonstrated. Indeed, for SIS1 (I_C = 895 nA), the experimentally observed lifetime is even shorter than that predicted by theory; see **Figure 5b**, the curve at 17 mK. For the SIS2 sample (I_C = 270 nA), the theoretical expectations are consistent with the experimental observations; see Figure 5d, the curve at 17 mK. A visible improvement in the lifetime is observed for SIS3 only (I_C = 87 nA); see **Figure 5f**, the curves at 17 and 13 mK. In spite of the fact that the quantum PD regime is observed here, it does not seriously improve the detector's performance. For instance, for the same lifetime of 5 s, the difference between the bias current predicted using MQT theory and the experimentally derived value is 1 nA only. This is not sufficient since the photon-induced current pulse itself is about 20 nA; see below.

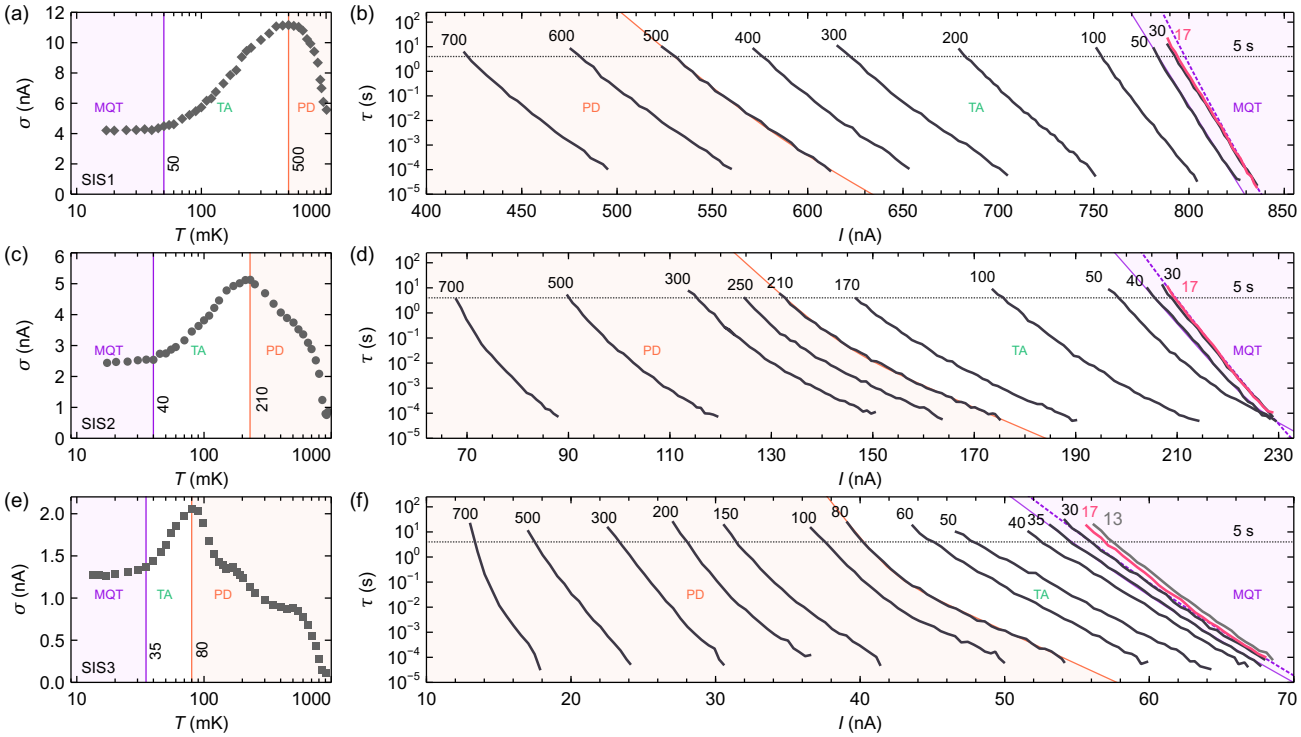

Figure 5 • The experimental data at different temperatures. The standard deviations in the switching currents (**left**) and lifetimes (**right**) for different sample temperatures (marked in mK above each curve). For clarification, the maximum critical current for a specific temperature can be taken as the value of the current at the point on the lifetime curve with the minimum τ value, which is approximately equal to $\langle I_{sw} \rangle(T)$; see **Figure 4**. (**a**,**b**) SIS1; (**c**,**d**) SIS2; (**e**,**f**) SIS3. The violet area corresponds to the MQT regime, the white area corresponds to the TA regime, and the orange area corresponds to the PD regime. The violet dashed line is the lifetime from MQT theory.

In the TA regime, the lifetimes, like the standard deviations, are traditionally described using the theory based on the Kramers expression $\tau_{TA}(T)$, Equation (1). However, this description does not apply to the PD regime. Indeed, $\sigma(T)$ decreases with an increasing temperature, reaching values even below the quantum saturation level at low temperatures; see **Figure 5c,e**. In parallel, the lifetime tilt $|d\tau/dI|$ also increases, indicating that a larger bias current can be used for the same lifetime τ.

3.3. Theoretical estimates of single-photon detection

Since we have determined the mean switching currents and lifetimes as a function of temperature and bias current for our CBJJs, we can analyze their performance as single-photon detectors. Assuming ideal coupling between the CBJJ and the incident photons, following [40], the photon-induced current can be estimated on account of the CBJJ losses, described by the quality factor Q. In this case, the photon energy $\hbar\omega_{ph}$ ($\omega_{ph}/2\pi$ is the photon frequency) is transferred to the energy of the SIS current; therefore, $I_{ph} = \sqrt{2\hbar\omega_{ph}L_J^{-1}\,(1+2\pi/Q)^{-1}}$, with the Josephson inductance $L_J = \hbar/(2e\sqrt{I_C^2 - I^2})$.

As follows from the expression above, the photon-induced current pulse amplitude differs for the investigated CBJJs since they have different parameters. Indeed, for the SIS1 sample, at a frequency of 10 GHz, the magnitude of the current pulse is about 50 nA, with weak temperature variation. For samples with lower critical currents, the magnitude of the current pulse depends on the temperature. For SIS2, this magnitude changes from 25 nA to 35 nA, and for SIS3, it changes from 12 nA to 22 nA when the temperature drops from 700 mK to 17 mK.

To demonstrate the temperature dependence of the lifetimes, we fixed a bias current shift $\Delta I = \langle I_{sw}\rangle - I$, taking it to be sufficiently smaller than the magnitude of the photon-induced current pulse to ensure proper switching of the detector. For each sample, we take the following values: SIS1—ΔI = 25 nA; SIS2—ΔI = 18 nA; SIS3—ΔI = 6 nA. The corresponding lifetime values, subtracted from **Figure 5b,d,f**, are presented in **Figure 6a**.

Furthermore, by choosing the desired dark count time, $\tau = 5$ s, as shown in **Figure 5b,d,f** with the dotted line, we can reconstruct the corresponding bias current values for each temperature. Selecting as an example a photon frequency of about 10 GHz [31] and taking into account the $I_C(T)$ dependence, we calculated the induced currents. Unambiguous switching of the detector occurs if $I + I_{ph} > \langle I_{sw}\rangle$. The results of our estimates are summarized in **Figure 6b**. The switching threshold is indicated in this figure by the dotted line.

The switching characteristics of a CBJJ between the zero- and finite-voltage states in the phase diffusion regime, presented in **Figure 6**, are quite unusual. While for the sample with a higher critical current (SIS1, I_C = 895 nA), both the lifetime and the total switching current $(I + I_{ph})/\langle I_{sw}\rangle$ decrease with a rise in temperature, as expected, these characteristics for samples with lower critical currents exhibit non-monotonic behavior. A decrease in the lifetime and the total switching current at temperatures slightly above the crossover temperature between the MQT and TA regimes is "compensated" for by an increase in these values in the PD regime. Importantly, for samples with lower critical currents, this increase is more pronounced. This observation is counter-intuitive. Indeed, as the critical current I_C decreases, the well depth of the washboard potential becomes smaller, since $E_J \sim I_C$; see **Figure 1a**. Automatically, the ratio between the Josephson E_J and the thermal energies k_BT decreases. Consequently, the transition to the running (finite-voltage) state requires less thermal energy, which contradicts the experiment. Qualitatively, it can be explained as follows. With the increase in the temperature, the probability of an escaping particle becoming re-trapped in an adjacent potential well increases. Since the threshold detector only recognizes the difference between the zero- and finite-voltage states, it ignores noise-induced escapes, unless these escapes produce a finite voltage, which improves the overall detector performance. A theoretical explanation of this effect requires further study involving outlining the roles of damping and temperature in the CBJJ's dynamics.

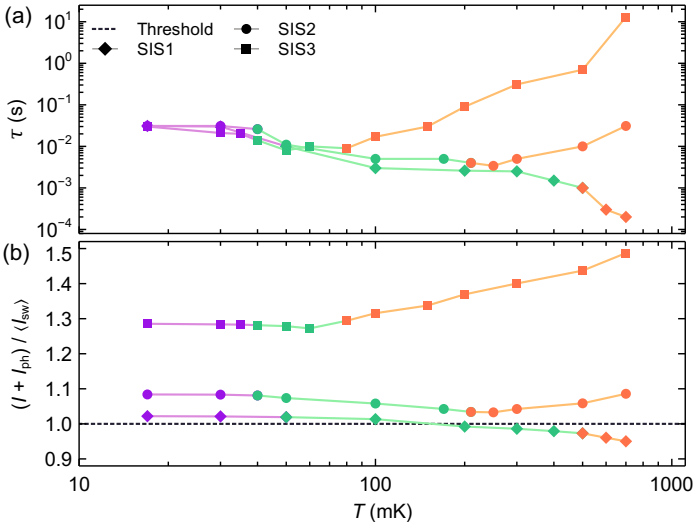

Figure 6 • Theoretical estimates of the single-photon detection efficiency. (**a**) The lifetimes with a fixed shift in the bias current ($I = \langle I_{sw}\rangle - \Delta I$) for each sample: SIS1—$\Delta I$ = 25 nA; SIS2—ΔI = 18 nA; SIS3—ΔI = 6 nA. (**b**) The normalized total current $(I + I_{ph})/\langle I_{sw}\rangle$ due to the absorption of a 10 GHz photon versus the temperature of the samples. The threshold is a normalized critical current. The violet part of the curve corresponds to the MQT regime, the green part corresponds to the TA regime, and the orange part corresponds to the PD regime.

3.4. Photon detection experiments

Based on the above-described reasoning for the possible microwave photon detection at sub-K temperatures, we performed measurements as follows. The external microwave signal generated by the synthesizer is strongly attenuated, thus decaying into a stream of photons obeying Poisson statistics [47, 67, 68].

The attenuating stages include the synthesizer's built-in attenuator, with a power adjustment range of 1–30 dB; a 10 dB attenuator after the synthesizer output; and 60dB attenuators distributed along the coaxial line inside the refrigerator. The signal is emitted by a loop antenna weakly coupled to the sample (**Figure 2**). This technique for detecting microwave photons with power calibration using photon-assisted tunnelling (PAT) steps at the IVC branch [69, 70] was described in detail in [21, 47].

After the signal has been calibrated using the PAT steps, we use the built-in attenuator of the synthesizer and collect the switching probability versus the attenuated power—see **Figure 7a**—thus transferring to rare photon flux at the scale of the detector's switch-

ing time, in the order of 1 ns, while the detector's dead time is restricted by the RC filters used and is about 1 ms. Here, due to the PAT steps—see **Figure 7b**—the 20 dBm of power output by the synthesizer corresponds to an accepted power of 65 fW at 17 mK and 48 fW at 700 mK, and the curves in **Figure 7a** are normalized, respectively. Therefore, the accepted power slightly decreases due to the suppressed gap.

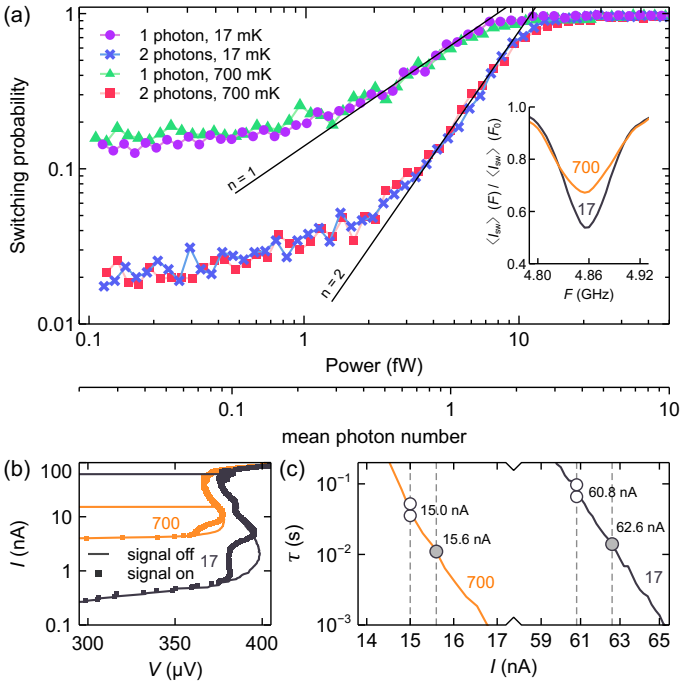

Figure 7 • (**a**) The switching probability versus the normalized AC power of 4.86 GHz single- and double-photon detection at 17 mK and 700 mK using SIS3. The solid line n = 1 corresponds to the single-photon detection tilt, and the solid line n = 2 corresponds to the double-photon detection tilt. The inset is the renormalized average of the switching current vs. the microwave signal's frequency. (**b**) The IVC for SIS3 with a microwave signal (square markers, PAT steps) and without a microwave signal (solid curves) at temperatures of 17 mK (black) and 700 mK (orange). (**c**) The lifetime values corresponding to the bias currents where single- and double-photon detection occurs for temperatures of 17 mK and 700 mK. Gray markers correspond to single-photon detection, and white markers correspond to double-photon detection.

The microwave signal frequency is set to 4.86 GHz. This is due to the fact that for a plasma frequency close to 10 GHz for the SIS3 sample, the maximal response is expected to be approximately half the plasma's frequency [42, 44], which is confirmed by the measurements of the SCDs versus the frequency at fixed output powers of 17 mK and 700 mK, shown in the inset in **Figure 7a**. It should be noted that the detector considered has a rather narrow bandwidth, not exceeding 3% of the central frequency, therefore decreasing the effect of the background photons. Here, the background photons appear from the surrounding sample holder, representing a cavity, so only thermal photons from resonant modes are excited, as investigated in [21].

The detection of microwave photons at two temperatures of 17 mK and 700 mK is shown in **Figure 7a**. Decreasing the bias current value, we increase the potential barrier height and can change the number of detected photons. One can see that the switching probability curves versus power, both at 17 mK and 700 mK, have tilts corresponding to single-photon and double-photon detection [68] (one and two orders of probability to one order of power, respectively). Therefore, for 5 GHz microwave photons, we achieve approximately 15% efficiency in single-photon detection even at sub-K temperatures. It should be noted that the dark count floor (the nearly constant part of the switching probability curves close to the 0.1 level) is almost the same for both 700 mK and 17 mK temperatures. The weak temperature dependence of the detector's performance observed is fully consistent with the analysis presented above.

4. Conclusions

We have experimentally demonstrated single- and double-photon sensing at ≈5 GHz by making use of a threshold detector, based on Al-made Josephson junctions with relatively low critical currents, exhibiting a phase diffusion regime. For double-photon detection, the characteristics of the detector obtained are quite impressive—with a dark count time τ of 0.1s, its efficiency is 90%. However, for single-photon detection, the parameters obtained are not so attractive: $\tau \approx 0.01$s, and the efficiency is 15%. Nevertheless, it is important to note that for a particular sample with a dominating phase diffusion regime, these numbers are almost temperature-independent. This means that the main mechanism limiting the detector's performance is "unwanted" photons rather than thermal fluctuations. Further research is required to characterize the source of such uncontrolled photons. These results are important for axion search experiments in the range of 5–25 GHz (20–100 μeV) [35]. In this case, typical experiments with a cavity, placed inside a strong magnet, are assumed [23], where the signal from a cavity is fed to the detector by a coaxial line. The operation of the detector at 0.7 K allows the detector to be moved from a dilution plate to a condensing 0.7 K plate in a fridge. This allows the distance from the magnet to be increased, which is usually located just below the dilution plate, thus reducing the effect of a high magnetic field on the detector.

Acknowledgments

The authors wish to thank A.A. Yablokov for writing the automated Python-based software and I.V. Rakut' for fabricating the sample holder.

Funding

This research was funded by the Russian Science Foundation, grant number 19-79-10170.

Author contributions

Conceptualization, A.L.P., D.A.L., and E.V.I.; methodology, A.L.P., L.S.R. and D.A.L.; software, D.A.L.; validation D.A.L., A.L.P., L.S.R., A.V.G. and A.V.C.; formal analysis D.A.L. and A.L.P.; investigation, D.A.L., A.L.P., L.S.R., A.V.G. and S.A.R.; resources A.V.G. and A.L.P.; data curation, D.A.L. and A.V.C.; writing—original draft preparation, D.A.L.; writing—review and editing, A.L.P. and E.V.I.; visualization, D.A.L.; supervision, E.V.I.; project administration, A.L.P.; funding acquisition, A.V.G. All authors have read and agreed to the published version of the manuscript.

Conflict of interest

The authors declare that they have no known competing financial interests or personal relationships that could have appeared to influence the work reported in this paper.

Data availability statement

The data supporting these findings are available within the article or upon request.

Institutional review board statement

Not applicable.

Informed consent statement

Not applicable.

Additional information

Received: 2025-04-22

Accepted: 2025-06-16

Published: 2025-06-27

Academia Quantum papers should be cited as *Academia Quantum 2025*, ISSN 3064-979X, https://doi.org/10.20935/AcadQuant7780. The journal's official abbreviation is *Acad. Quant*.

Publisher's note

Copyright

References

1. Esmaeil-Zadeh I, Chang J, Los JWN, Gyger S, Elshaari AW, Steinhauer S, et al. Superconducting nanowire single-photon detectors: a perspective on evolution, state-of-the-art, future developments, and applications. Appl Phys Lett. 2021;118(19):191102. doi: 10.1063/5.0045990
2. Kovalyuk VV, Venediktov IO, Sedykh KO, Svyatodukh SS, Hydyrova S, Moiseev KM, et al. Waveguide integrated superconducting single-photon detector for photonic and ion quantum processors and neuromorphic computing. Radiophys Quantum Electron. 2024;66(11):839–92. doi: 10.1007/s11141-024-10340-9
3. Irwin KD. SQUIDs and transition-edge sensors. J Supercond Novel Magn. 2021;34(6):1601–6. doi: 10.1007/s10948-020-05730-9
4. Fink CW, Watkins SL, Aramaki T, Brink PL, Camilleri J, Defay X, et al. Performance of a large area photon detector for rare event search applications. Appl Phys Lett. 2021;118(2):022601. doi: 10.1063/5.0032372
5. SuperCDMS Collaboration. Light dark matter search with a high-resolution athermal phonon detector operated above ground. Phys Rev Lett. 2021;127(6):061801. doi: 10.1103/PhysRevLett.127.061801
6. Johnson BR, Reed MD, Houck AA, Schuster DI, Bishop LS, Ginossar E, et al. Quantum non-demolition detection of single microwave photons in a circuit. Nat Phys. 2010;6(9):663–7. doi: 10.1038/nphys1710
7. Inomata K, Lin Z, Koshino K, Oliver WD, Tsai JS, Yamamoto T, et al. Single microwave-Photon detector using an artificial λ-type three-level system. Nat Commun. 2016;7:12303. doi: 10.1038/ncomms12303
8. Besse JC, Gasparinetti S, Collodo MC, Walter T, Kurpiers P, Pechal M, et al. Single-Shot quantum nondemolition detection of individual itinerant microwave photons. Phys Rev X. 2018;8(2):021003. doi: 10.1103/PhysRevX.8.021003
9. Royer B, Grimsmo AL, Choquette-Poitevin A, Blais A. Itinerant microwave photon detector. Phys Rev Lett. 2018;120(20):203602. doi: 10.1103/PhysRevLett.120.203602
10. Kono S, Koshino K, Tabuchi Y, Noguchi A, Nakamura Y. Quantum non-demolition detection of an itinerant microwave photon. Nat Phys. 2018;14(6):546–9. doi: 10.1038/s41567-018-0066-3
11. Lescanne R, Deléglise S, Albertinale E, Régade U, Capelle T, Ivanov E, et al. Irreversible qubit-photon coupling for the detection of itinerant microwave photons. Phys Rev X. 2020;10(2):021038. doi: 10.1103/PhysRevX.10.021038
12. Albertinale E, Balembois L, Billaud E, Ranjan V, Flanigan D, Schenkel T, et al. Detecting spins by their fluorescence with a microwave photon counter. Nature. 2021;600(7889):434–8. doi: 10.1038/s41586-021-04076-z
13. Grimsmo AL, Royer B, Kreikebaum JM, Ye Y, O'Brien K, Siddiqi I, et al. Quantum Metamaterial for broadband detection of single microwave photons. Phys Rev Appl. 2021;15(3):034074. doi: 10.1103/PhysRevApplied.15.034074
14. Dixit AV, Chakram S, He K, Agrawal A, Naik RK, Schuster DI, et al. Searching for dark matter with a superconducting qubit. Phys Rev Lett. 2021;126(14):141302. doi: 10.1103/PhysRevLett.126.141302

15. Khan W, Potts PP, Lehmann S, Thelander C, Dick KA, Samuelsson P, et al. Efficient and continuous microwave photoconversion in hybrid cavity-semiconductor nanowire double quantum dot diodes. Nat Commun. 2021;12:5130. doi: 10.1038/s41467-021-25446-1

16. Balembois L, Travesedo J, Pallegoix L, May A, Billaud E, Villiers M, et al. Cyclically operated microwave single-photon counter with sensitivity of $10^{-22}\,\mathrm{W}/\sqrt{\mathrm{hz}}$. Phys Rev Appl. 2024;21:014043. doi: 10.1103/PhysRevApplied.21.014043

17. Haldar S, Zenelaj D, Potts PP, Havir H, Lehmann S, Dick KA, et al. Microwave power harvesting using resonator-coupled double quantum dot photodiode. Phys Rev B. 2024;109(8):L081403. doi: 10.1103/PhysRevB.109.L081403

18. Petrovnin K, Wang J, Perelshtein M, Hakonen P, Paraoanu GS. Microwave photon detection at parametric criticality. PRX Quantum. 2024;5(2):020342. doi: 10.1103/prxquantum.5.020342

19. Martinis JM, Nam S, Aumentado J, Urbina C. Rabi oscillations in a large josephson-junction qubit. Phys Rev Lett. 2002;89(11):117901. doi: 10.1103/physrevlett.89.117901

20. Barone A, Paternò G. Physics and Applications of the Josephson Effect. New York (NY): John Wiley & Sons; 1982.

21. Pankratov AL, Gordeeva AV, Chiginev AV, Revin LS, Blagodatkin AV, Crescini N, et al. Detection of single-mode thermal microwave photons using an underdamped josephson junction. Nat Commun. 2025;16:3457. doi: 10.1038/s41467-025-56040-4

22. Lamoreaux SK, van Bibber KA, Lehnert KW, Carosi G. Analysis of single-photon and linear amplifier detectors for microwave cavity dark matter axion searches. Phys Rev D. 2013;88:035020. doi: 10.1103/physrevd.88.035020

23. Sikivie P. Invisible axion search methods. Rev Mod Phys. 2021;93(1):015004. doi: 10.1103/revmodphys.93.015004

24. Braine TB, Cervantes R, Crisosto N, Du N, Kimes S, Rosenberg LJ, et al. Extended search for the invisible axion with the axion dark matter experiment. Phys Rev Lett. 2020;124:101303. doi: 10.1103/PhysRevLett.124.101303

25. Crescini N, Alesini D, Braggio C, Carugno G, D'Agostino D, Di Gioacchino D, et al. Axion Search with a quantum-limited ferromagnetic haloscope. Phys Rev Lett. 2020;124(17):171801. doi: 10.1103/PhysRevLett.124.171801

26. Kwon O, Lee D, Chung W, Ahn D, Byun HS, Caspers, F, et al. First Results from an axion haloscope at CAPP around 10.7 μeV. Phys Rev Lett. 2021;126(19):191802. doi: 10.1103/PhysRevLett.126.191802

27. Keller A, O'Brien S, Kamdar A, Rapidis NM, Leder AF, van Bibber K. A Model-independent Radio telescope dark matter search. Astrophys J. 2022;927(1):71. doi: 10.3847/1538-4357/ac4d93

28. Adair CM, Altenmüller K, Anastassopoulos V, Arguedas Cuendis S, Baier J, Barth K et al. Search for dark matter axions with cast-capp. Nat Commun. 2022;13(1):6180. doi: 10.1038/s41467-022-33913-6

29. Yi AK, Ahn S, Kutlu Ç, Kim J, Ko B.R, Ivanov B.I, et al. Axion dark matter search around 4.55 μeV with dine-fischler-srednicki-zhitnitskii sensitivity. Phys Rev Lett. 2023;130(7):071002. doi: 10.48550/arXiv.2210.10961

30. Sushkov AO. Quantum science and the search for axion dark matter. Phys Rev X Quantum. 2023;4(1):020101. doi: 10.1103/prxquantum.4.020101

31. Graham E, Ghosh S, Zhu Y, Bai X, Cahn SB, Durcan E, et al. Rydberg-atom-based single-photon detection for haloscope axion searches. Phys Rev D. 2024;109(3):032009. doi: 10.1103/PhysRevD.109.032009

32. Uchaikin SV, Kim J, Kutlu C, Ivanov BI, Kim J, van Loo AF, et al. Josephson parametric amplifier based quantum noise limited amplifier development for axion search experiments in CAPP. Front Phys. 2024;12:1437680. doi: 10.3389/fphy.2024.1437680

33. Ahn S, Kim J, Ivanov BI, Kwon O, Byun H, van Loo AF, et al. Extensive Search for axion dark matter over 1 GHz with CAPP'S main axion experiment. Phys Rev X. 2024;14(3):031023. doi: 10.1103/PhysRevX.14.031023

34. GigaBREAD Collaboration. First axionlike particle results from a broadband search for wavelike dark matter in the 44 to $52\ \mu$eV range with a coaxial dish antenna. Phys Rev Lett. 2025;134(17):171002. doi: 10.48550/arXiv.2501.17119

35. Buschmann M, Foster JW, Hook A, Peterson A, Willcox DE, Zhang W, et al. Dark matter from axion strings with adaptive mesh refinement. Nat Commun. 2022;13:1049. doi: 10.48550/arXiv.2108.05368

36. Chen YF, Hover D, Sendelbach S, Maurer L, Merkel ST, Pritchett EJ, et al. Microwave photon counter based on josephson junctions. Phys Rev Lett. 2011;107(21):217401. doi: 10.1103/PhysRevLett.107.217401

37. Peropadre B, Romero G, Johansson G, Wilson CM, Solano E, García-Ripoll JJ. Approaching perfect microwave photodetection in circuit QED. Phys Rev A. 2011;84(6):063834. doi: 10.1103/physreva.84.063834

38. Addesso P, Filatrella G, Pierro V. Characterization of escape times of Josephson junctions for signal detection. Phys Rev E. 2012;85(1):016708. doi: 10.1103/physreve.85.016708

39. Poudel A, McDermott R, Vavilov MG. Quantum efficiency of a microwave photon detector based on a current-biased Josephson junction. Phys Rev B. 2012;86(17):174506. doi: 10.1103/physrevb.86.174506

40. Kuzmin LS, Sobolev AS, Gatti C, Di Gioacchino D, Crescini N, Gordeeva A, et al. Single photon counter based on a josephson junction at 14 GHz for searching galactic axions. IEEE Trans Appl Supercond. 2018;28(7):2400505. doi: 10.1109/tasc.2018.2850019

41. Piedjou Komnang AS, Guarcello C, Barone C, Gatti C, Pagano S, Pierro V, et al. Analysis of Josephson junctions switching time distributions for the detection of single microwave photons. Chaos Solitons Fractals. 2021;142:110496. doi: 10.1016/j.chaos.2020.110496

42. Yablokov AA, Glushkov EI, Pankratov AL, Gordeeva AV, Kuzmin LS, Il'ichev EV. Resonant response drives sensitivity of Josephson escape detector. Chaos Solitons Fractals. 2021;148:111058. doi: 10.1016/j.chaos.2021.111058

43. Golubev DS, Il'ichev EV, Kuzmin LS. Single-photon detection with a Josephson Junction coupled to a resonator. Phys Rev Appl. 2021;16(1):014025. doi: 10.1103/physrevapplied.16.014025

44. Ladeynov DA, Egorov DG, Pankratov AL. Stochastic versus dynamic resonant activation to enhance threshold detector sensitivity. Chaos Solitons Fractals. 2023;171:113506. doi: 10.1016/j.chaos.2023.113506

45. Stanisavljević O, Philippe JC, Gabelli J, Aprili M, Estève J, Basset J. Efficient Microwave photon-to-electron conversion in a high-impedance quantum circuit. Phys Rev Lett. 2024;133(7):076302. doi: 10.1103/physrevlett.133.076302

46. He JX, Ouyang PH, Chai YQ, Chang H, He Q, Wei LF. Experimental demonstrations of Josephson threshold detectors for broadband microwave photons detection. Appl Phys Lett. 2025;126(20):202601. doi: 10.1063/5.0259463

47. Pankratov AL, Revin LS, Gordeeva AV, Yablokov AA, Kuzmin LS, Ilichev EV. Towards a microwave single-photon counter for searching axions. NPJ Quantum Information. 2022;8:61. doi: 10.1038/s41534-022-00569-5

48. Kautz RL, Martinis JM. Noise-affected I-V curves in small hysteretic Josephson junctions. Phys Rev B. 1990;42(16):9903–37. doi: 10.1103/PhysRevB.42.9903

49. Koval Y, Fistul MV, Ustinov AV. Enhancement of Josephson phase diffusion by microwaves. Phys Rev Lett. 2004;93(8):087004. doi: 10.1103/physrevlett.93.087004

50. Kivioja JM, Nieminen TE, Claudon J, Buisson O, Hekking FWJ, Pekola JP. Observation of transition from escape dynamics to underdamped phase diffusion in a Josephson junction. Phys Rev Lett. 2005;94(24):247002. doi: 10.1103/physrevlett.94.247002

51. Männik J, Li S, Qiu W, Chen W, Patel V, Han S, et al. Crossover from Kramers to phase-diffusion switching in moderately damped Josephson junctions. Phys Rev B. 2005;71(22):220509. doi: 10.1103/physrevb.71.220509

52. Krasnov VM, Bauch T, Intiso S, Hürfeld E, Akazaki T, Takayanagi H, et al. Collapse of thermal activation in moderately damped josephson junctions. Phys Rev Lett. 2005;95(15):157002. doi: 10.1103/physrevlett.95.157002

53. Fenton JC, Warburton PA. Monte Carlo simulations of thermal fluctuations in moderately damped Josephson junctions: Multiple escape and retrapping, switching- and return-current distributions, and hysteresis. Phys Rev B. 2008;78(5):054526. doi: 10.1103/physrevb.78.054526

54. Yoon Y, Gasparinetti S, Möttönen M, Pekola JP. Capacitively enhanced thermal escape in underdamped josephson junctions. J Low Temp Phys. 2011;163(3):164–9. doi: 10.1007/s10909-011-0344-2

55. Yu HF, Zhu XB, Peng ZH, Tian Y, Cui DJ, Chen GH, et al. Quantum Phase diffusion in a small underdamped josephson junction. Phys Rev Lett. 2011;107(6):067004. doi: 10.1103/physrevlett.107.067004

56. Longobardi L, Massarotti D, Rotoli G, Stornaiuolo D, Papari G, Kawakami A, et al. Thermal hopping and retrapping of a Brownian particle in the tilted periodic potential of a NbN/MgO/NbN Josephson junction. Phys Rev B. 2011;84(18):184504. doi: 10.1103/physrevb.84.184504

57. Longobardi L, Massarotti D, Stornaiuolo D, Galletti L, Rotoli G, Lombardi F, et al. Direct Transition from quantum escape to a phase diffusion regime in YBaCuO biepitaxial josephson junctions. Phys Rev Lett. 2012;109(5):050601. doi: 10.1103/physrevlett.109.050601

58. Revin LS, Pankratov AL, Gordeeva AV, Yablokov AA, Rakut IV, Zbrozhek VO, et al. Microwave photon detection by an Al Josephson junction. Beilstein J Nanotechnol. 2020;11:960–5. doi: 10.3762/bjnano.11.80

59. Pankratov AL, Ladeynov DA, Revin LS, Gordeeva AV, Ilichev EV. Quantum and phase diffusion crossovers in small Al Josephson junctions. Chaos Solitons Fractals. 2024;184:114990. doi: 10.1016/j.chaos.2024.114990

60. Voss RF, Webb RA. Macroscopic quantum tunneling in 1-μm Nb Josephson Junctions. Phys Rev Lett. 1981;47(4):265–8. doi: 10.1103/physrevlett.47.265

61. Martinis JM, Grabert H. Thermal enhancement of macroscopic quantum tunneling: derivation from noise theory. Phys Rev B. 1988;38(4):2371–9. doi: 10.1103/physrevb.38.2371

62. Blackburn JA, Cirillo M, Grønbach-Jensen N. A survey of classical and quantum interpretations of experiments on Josephson junctions at very low temperatures. Phys Rep. 2016;611:1–33. doi: 10.1016/j.physrep.2015.10.010

63. Pankratov AL, Salerno M. Adiabatic approximation and parametric stochastic resonance in a bistable system with periodically driven barrier. Phys Rev E. 2000;61(2):1206–10. doi: 10.1103/physreve.61.1206

64. Pankratov AL, Gordeeva AV, Revin LS, Ladeynov DA, Yablokov AA, Kuzmin LS. Approaching microwave photon sensitivity with Al Josephson junctions. Beilstein J Nanotechnol. 2022;13(1):582–9. doi: 10.3762/bjnano.13.50

65. Barends R, Wenner J, Lenander M, Chen Y, Bialczak RC, Kelly J, et al. Minimizing quasiparticle generation from stray infrared light in superconducting quantum circuits. Appl Phys Lett. 2011;99(11):113507. doi: 10.1063/1.3638063

66. Kurkijärvi J. Intrinsic fluctuations in a superconducting ring closed with a josephson junction. Phys Rev B. 1972;6(8):832. doi: 10.1103/physrevb.6.832

67. Fox M. Quantum Optics: An Introduction. Oxford: OUP; 2006.

68. Goltsman GN, Okunev O, Chulkova G, Lipatov A, Semenov A, Smirnov K, et al. Picosecond superconducting single-photon optical detector. Appl Phys Lett. 2001;79(6):705–7. doi: 10.1063/1.1388868

69. Tien PK, Gordon JP. Multiphoton process observed in the interaction of microwave fields with the tunneling between superconductor films. Phys Rev. 1963;129(2):647–51. doi: 10.1103/physrev.129.647

70. Tucker JR, Feldman MJ. Quantum detection at millimeter wavelengths. Rev Mod Phys. 1985;57(4):1055–113. doi: 10.1103/RevModPhys.57.1055